Magnetic field dependence of the many-electron states in a magnetic quantum dot: The ferromagnetic-antiferromagnetic transition

Nga T. T. Nguyen* and F. M. Peeters†
Departement Fysica, Universiteit Antwerpen, Groenenborgerlaan 171, B-2020 Antwerpen, Belgium
(Received 17 January 2008; revised manuscript received 4 June 2008; published 25 July 2008)

The electron-electron correlations in a many-electron ($N_e=1,2,\ldots,5$) quantum dot confined by a parabolic potential is investigated in the presence of a single magnetic ion and a perpendicular magnetic field. We obtained the energy spectrum and calculated the addition energy which exhibits cusps as a function of the magnetic field. The vortex properties of the many-particle wave function of the ground state are studied and for large magnetic fields are related to composite fermions. The position of the impurity influences strongly the spin-pair-correlation function when the external field is large. In a small applied magnetic field, the spin-exchange energy together with the Zeeman terms leads to a ferromagnetic-antiferromagnetic (FM-AFM) transition. When the magnetic ion is shifted away from the center of the quantum dot, a remarkable re-entrant AFM-FM-AFM transition is found as a function of the strength of the Coulomb interaction. Thermodynamic quantities such as the heat capacity, the magnetization, and the susceptibility are also studied. The cusps in the energy levels show up as peaks in the heat capacity and the susceptibility.

DOI: 10.1103/PhysRevB.78.045321 PACS number(s): 73.21.La, 75.30.Hx, 75.75.+a, 75.50.Pp

I. INTRODUCTION

Magnetically doped quantum dots[1] have attracted considerable theoretical and experimental interests over the last two decades. Diluted magnetic II-VI and III-V semiconductor (DMS) quantum dots were fabricated with single-electron control.[2,3] A rich variety of different magnetic and optical properties were discovered.[4–10] In such structures one can explore the physical properties coming from intercarrier interactions and the interaction of the carriers with the magnetic ion. This system promises to be relevant for future quantum computing devices, where for instance the spin of the magnetic ion is used as a quantum bit. More recently, electrically active devices were fabricated in which a single manganese ion is inserted into a single quantum dot[11] with control of the amount of charge in the quantum dot and consequently the possibility of control of magnetism of single Mn-doped quantum dots.

The investigation of the exact electronic structure of a two-dimensional quantum dot confined by a parabolic potential containing several electrons and a single magnetic impurity (in this paper Mn^{2+}) in the presence of an applied magnetic field is a new topic. In a recent investigation,[12] a three-dimensional (3D) Cd(Mn)Se quantum dot containing several electrons, where only the low-energy levels of the single-electron problem were taken into account, was investigated in the presence of a magnetic field. Here we will extend this work and include all relevant energy levels in order to obtain a convergent solution for the ground state (and also the excited spectrum) of the system.

It is known that in the absence of a magnetic ion, an external magnetic field is able to change the spin-polarized state of weakly interacting N_e electrons in a quantum dot in such a way that in the ground state it maximizes the total spin of the system: i.e., $S=N_e/2$. If the interparticle interaction is strong, even without an applied magnetic field the electrons may already be polarized. However, with increasing magnetic field and in the case that the interparticle interaction is strong, the total spin of the system can be unusually reduced by the magnetic field.[13]

In the present study, we investigate theoretically the few-electron two-dimensional confined quantum dot system that contains a single magnetic ion in the presence of an external magnetic field taking into account a sufficient large number of single-particle orbitals such that numerical "exact" results are obtained. We explore how sensitive the whole system is to the position of the magnetic ion in the quantum dot and to the presence of a magnetic field. Moreover, we investigate the competition between the following three energies: (i) the interaction of the magnetic ion with the electrons, (ii) the interaction of the magnetic ion with the magnetic field, and (iii) the interaction of the external field with the electrons. These terms affect the spin polarization of the N_e electrons in the quantum dot.

Explicit studies of an N_e-correlated-electron system interacting with a single magnetic ion in nonzero magnetic field are very rare in the literature. Recent theoretical[10,12,14,15] and experimental works[11] focused either on a small number of electrons using the exact diagonalization approach at zero field (Refs. 14 and 15) for a two-dimensional (2D) quantum dot or at nonzero field[12] including only the lowest single-particle states for a 3D system or on the exciton states relevant for optical spectroscopy of self-assembled magnetically doped quantum dots.[10,11]

Here, we will examine thoroughly the exact properties of the system containing several correlated electrons and a single magnetic impurity in the presence of a magnetic field. In our numerical "exact" diagonalization approach, we include an arbitrary number of single-particle states to guarantee the accuracy of our results. We investigate the influence of the strength of the interparticle interaction and the position of the magnetic ion on the ground state of the system. We predict the interesting phenomenon that the magnetic ion ferromagnetically couples with the electrons in a region below a critical magnetic field and antiferromagnetically with the electrons above this critical field. Thermodynamic properties such as magnetization, susceptibility, and heat capacity are investigated as a function of magnetic field and temperature.

This paper is organized as follows: Section II introduces the model and the numerical method. In Sec. III, we present

our numerical results for the many-particle ground state and investigate correlations through the appearance of vortices in the many-electron wave function. Section IV addresses the many-particle spectrum and in Sec. V we present results for different thermodynamic quantities. Our discussion and conclusions are presented in Sec. VI.

II. THEORETICAL MODEL

A quantum dot containing N_e electrons with spins $\vec{s_i}$ confined by a parabolic potential and interacting with a single magnetic ion (Mn^{2+}) with spin $\vec{M}$ and a magnetic field is described by the following Hamiltonian:

$$\hat{H} = \sum_{i=1}^{N_e} \left\{ \frac{1}{2m^*}[-i\hbar\vec{\nabla}_{\vec{r}_i} + e\vec{A}(\vec{r}_i)]^2 + \frac{1}{2}m^*\omega_0^2\vec{r}_i^{\,2} \right\} + \sum_{i<j=1}^{N_e} \frac{e^2}{4\pi\epsilon_0\epsilon|\vec{r}_i - \vec{r}_j|} + \frac{1}{2}\hbar\omega_c(g_e m^* S_z + g_{\mathrm{Mn}} m^* M_z) - J_c \sum_{i=1}^{N_e} \vec{s}_i \cdot \vec{M}\,\delta(\vec{r}_i - \vec{R}). \quad (1)$$

The vector potential $\vec{A}$ is taken in the symmetric gauge: $\vec{A} = B/2(-y,x,0)$, where the magnetic field $\vec{B}$ points perpendicular to the plane of the interface. The confinement frequency ω_0 is related to the confinement length by $l_0 = \sqrt{\hbar/m^*\omega_0}$. g_e and g_{Mn} are the Landé g factors of the host semiconductor and the magnetic ion, respectively. The dimensionless Coulomb strength is defined as $\lambda_C = l_0/a_B^*$, with $a_B^* = 4\pi\epsilon_0\epsilon\hbar^2/m^*e^2$ as the effective Bohr radius. The cyclotron frequency is $\omega_c = eB/m^*$. L_z, S_z, and M_z are the projections of the total angular momenta of the electrons, their spins, and the magnetic ion in the direction of the magnetic field. The electrons and the magnetic impurity in the quantum dot interact via the contact exchange interaction with strength J_c.

We use the set of parameters[7,14] that is applicable to Cd(Mn)Te which is a II(Mn)VI quantum dot with typical lateral size of about tens of nanometers. The dielectric constant $\epsilon = 10.6$, effective mass $m^* = 0.106m_0$, $a_B^* = 52.9$ Å, $g_e = -1.67$, $g_{\mathrm{Mn}} = 2.02$, $J_c = 1.5 \times 10^3$ meV Å^2, and l_0 is about tens of nanometers ($\hbar\omega_0$ corresponding to tens of meV). For example, $\hbar\omega_0 = 51.32$ meV gives $l_0 = 26.45$ Å.

We rewrite the Hamiltonian in the second-quantized form:

$$\hat{H} = \sum_{i,\sigma} E_{i,\sigma} c_{i,\sigma}^+ c_{i,\sigma} + \frac{1}{2} \sum_{ijkl\sigma\sigma'} \langle i,j|V_0|k,l\rangle c_{i,\sigma}^+ c_{j,\sigma'}^+ c_{k,\sigma'} c_{l,\sigma} + \frac{1}{2}\hbar\omega_c(g_e m^* S_z + g_{\mathrm{Mn}} m^* M_z) - \sum_{ij} \frac{1}{2} J_{ij}(\vec{R})[(c_{i,\uparrow}^+ c_{j,\uparrow} - c_{i,\downarrow}^+ c_{j,\downarrow})M_z + c_{i,\uparrow}^+ c_{j,\downarrow} M^- + c_{i,\downarrow}^+ c_{j,\uparrow} M^+], \quad (2)$$

where the first term is the single-particle energies $E_{i,\sigma}$ for an electron in state i with spin σ and the second term is the Coulomb interaction. The third term is the electron and magnetic ion Zeeman energy. The last sum is the electron-Mn interaction, in which the first term describes the difference between the number of spin-up and spin-down electrons and the last two terms describe the energy gained by flipping the electron spin alongside with flipping the spin of the magnetic ion. M_z M^+, and M^- are the z-projection raising and lowering operators, respectively, of the magnetic ion spin (we consider Mn ions which have a spin of size $M = 5/2$).

The single-particle states in a parabolic confinement potential define a complete basis of Fock-Darwin orbitals $\phi_{nl}(\vec{r})$ and spin functions $\chi_\sigma(\vec{s})$:

$$\phi_{nl\sigma}(\vec{r},\vec{s}) = \varphi_{nl}(\vec{r})\chi_\sigma(\vec{s}), \quad (3)$$

with the Fock-Darwin orbitals

$$\varphi_{nl}(\vec{r}) = \frac{1}{l_H}\sqrt{\frac{n!}{\pi(n+|l|)!}}\left(\frac{r}{l_H}\right)^{|l|} e^{-il\theta} e^{-r^2/2l_H^2} L_n^{|l|}(r^2/l_H^2). \quad (4)$$

In Hamiltonian (2), i denotes a set of quantum numbers $\{n,l\}$ with n,l as the radial and azimuthal quantum numbers, respectively. The effective length $l_H = \sqrt{\hbar/m^*\omega_H} = l_0/\alpha$ in the presence of a magnetic field is defined through the hybrid frequency $\omega_H = \omega_0\sqrt{1+(\omega_c/2\omega_0)^2}$, where $\alpha = \sqrt[4]{1+(\omega_c/2\omega_0)^2}$. The single-particle orbital energy is given by

$$E_{i,\sigma} = \hbar\omega_H(2n + |l| + 1) - \hbar\omega_c l/2. \quad (5)$$

The interaction parameters between the electrons and the magnetic ion in the quantum dot is expressed as

$$J_{ij}(\vec{R}) = J_c\varphi_i^*(\vec{R})\varphi_j(\vec{R}), \quad (6)$$

as a product of two Fock-Darwin orbitals calculated at the position of the magnetic ion.

We construct the many-particle wave function following the configuration-interaction (CI) method:

$$\Psi(\vec{x_1^*},\vec{x_2^*},\ldots,\vec{x_{N_e}^*},\vec{M}) = \sum_{k=1}^{N_C} C_k\Psi_k, \quad (7)$$

where Ψ_k is the kth state of the noninteracting many-electron wave function determined by N_e electrons with N_e different sets of quantum numbers (n,l,σ) and the single scatterer with one of the six states of the Mn. $\vec{x_i^*} = (\vec{r_i},\vec{s_i})$ stands for the coordinates and spin of a single electron. In second quantization representation, the state Ψ_k, which is a Slater determinant composed of single-electron states, can be translated into a ket vector $|k\rangle$ grouping a total of N_e electrons into $N_\uparrow$ electrons with the z component of spin up and $N_\downarrow = N_e - N_\uparrow$ electrons with the z component of spin down:

$$\Psi_k \Rightarrow |k\rangle = |c_{i_1\uparrow}^+, c_{i_2\uparrow}^+, \ldots, c_{i_{N\uparrow}}^+\rangle |c_{j_1\downarrow}^+, c_{j_2\downarrow}^+, \ldots, c_{j_{N\downarrow}}^+\rangle |M_z\rangle. \quad (8)$$

Here $i_{1\uparrow} \div i_{N\uparrow}$ and $j_{1\downarrow} \div j_{N\downarrow}$ are the indices of the single-electron states for which each index is a set of two quantum numbers (radial and azimuthal quantum numbers), as mentioned above.

The CI method, which is in principle exact if a sufficient number of states are included, is limited to a small number of electrons due to computational limitations. For a larger number of electrons and/or magnetic ions, other approaches that, e.g., are based on spin-density-functional theory (SDFT) us-

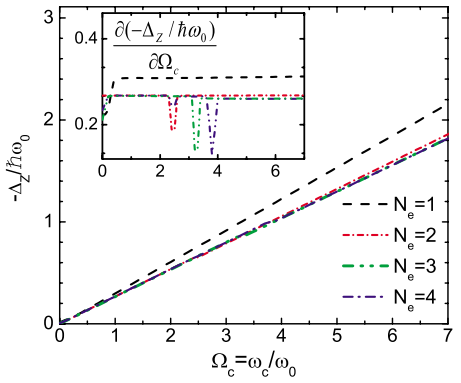

FIG. 1. (Color online) Total Zeeman energy for a quantum dot with different numbers of electrons. The magnetic ion is located at $(0.41l_0,0)$, and the Coulomb interaction strength λ_C=0.2. The inset is the first derivative of Δ_Z with respect to Ω_c that highlights the nonlinearity of Δ_Z in certain regions of the magnetic field.

ing, e.g., the local spin-density approximation (LSDA) as was used in Ref. 16 are able to handle a large number of electrons and/or magnetic ions. The LSDA is exact only in the case of the homogeneous electron gas, and in practice, works well also in most inhomogeneous systems. However, in really highly correlated few-particle systems as discussed in this paper, the LSDA might fail or be at least less accurate.

III. GROUND-STATE PROPERTIES

A. Zeeman energy

We first explore the magnetic field dependence of the total Zeeman energy:

$$\Delta_Z = E_C - E_{UC} = \Delta_Z^{\text{electron}} + \Delta_Z^{\text{Mn}} + (-\Delta_Z^{\text{exc}}), \tag{9}$$

which is the difference between energies in the presence and the absence of a magnetic ion. It consists of three terms: the difference between the Zeeman energies of the electrons, $\Delta_Z^{\text{electron}}$; the Zeeman energy describing the interaction of the magnetic ion having spin $\mathbf{M}=5/2$ with the magnetic field, Δ_Z^{Mn}; and the exchange interaction of the ion with the electrons, $-\Delta_Z^{\text{exc}}$. Δ_Z^{exc} is just the so-called local Zeeman splitting term as discussed in Ref. 15. This sum is basically the difference in the Zeeman energy of the electrons between the cases with and without a magnetic ion plus the energy contribution of the magnetic ion.

For N_e=1, we find a total Zeeman energy that appears linear in magnetic field. A similar linear behavior is also found in the cases with $N_e>1$ but with different slopes (see Fig. 1). Let us suppose, in Hamiltonian (1), that the contribution from the last term (the local Zeeman energy or the exchange interaction term) is zero. For instance this is the case where a magnetic ion is located at the center of the quantum dot with three electrons in the partially filled p shell, in which the first two electrons fully fill the s shell and the remaining one is in either of the orbitals of the p shell. Then a perfect linear behavior of the total Zeeman energy is found.

A closer look at Δ_Z gives us a slightly different picture, as provided by taking the derivative (see the inset of Fig. 1).

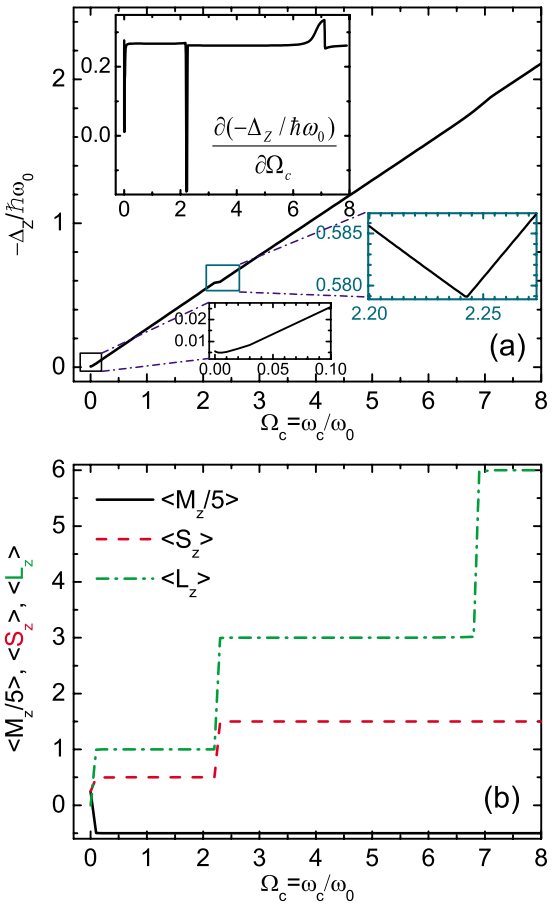

FIG. 2. (Color online) (a) Total Zeeman energy calculated for a three-electron quantum dot with the magnetic ion at $(0.5l_0,0)$ and λ_C=0.5. The upper inset is the first derivative of the main plot with respect to Ω_c to visualize more clearly the cusps. The lower inset is a zoom of the rectangular regions of the main plot. (b) The z projection of the total spin of the magnetic impurity (solid black curve), of the electrons (dashed red curve), and the total angular momentum (dash-dotted green curve).

Note that the total Zeeman term Δ_Z has pronounced cusps and the numbers and positions of these cusps are different for different numbers of electrons N_e. There exists one at Ω_c =2.6 for a two-electron quantum dot, one at Ω_c=3.4 for a three-electron quantum dot, and two at Ω_c=2.5 and 3.8 for the four-electron quantum dot, with the magnetic ion located at $(0.41l_0,0)$. The three-electron system exhibits a much richer behavior when we increase the Coulomb interaction strength to λ_C=0.5 as seen in Fig. 2(a), where we placed the magnetic ion at $(0.5l_0,0)$. Cusps, which are highlighted in the two insets of Fig. 2(a), appear when the total angular momentum and/or the total z projection of the spin of the electrons change abruptly with magnetic field. Note that the total Zeeman energy of a two-electron quantum dot in the presence of the magnetic ion does not produce a similar behavior due to the fact that the z projection of the total spin is zero, making the main contribution (from the Zeeman spin term of the Mn impurity) negligible.

The Coulomb strength and the position of the magnetic impurity affect the total Zeeman energy and influence the number and the position of the cusps. The first pronounced

cusp appears at lower magnetic field for larger Coulomb interaction strength. This is a consequence of the competition between the Coulomb energy and the energy gap of the single-particle problem. A larger Coulomb strength (smaller energy gap) leads to stronger electron-electron correlation and consequently the electrons are more clearly separated from each other. It results into a high probability of finding that the electrons occupy higher-energy states. That also means that the system transfers to a configuration with larger S_z and L_z at smaller applied field.

We also found that the ground-state energy is sensitive to the presence of the magnetic field. In zero magnetic field, the ground state receives contributions from many different configurations with z projection of the magnetic ion, M_z, from $-5/2$ to $5/2$. When a magnetic field is applied, the ground state favors states with projection of the spin of the magnetic ion down and the states with $M_z=-5/2$ give the main contribution to the ground state.

Figure 2(b) shows the average of the three quantities M_z, S_z, and L_z of the three-electron quantum dot as a function of the magnetic field for a Coulomb interaction strength $\lambda_C=0.5$. We realize that with increasing λ_C, the $\langle L_z\rangle$ ($\langle S_z\rangle$) exhibits jumps at smaller critical Ω_c (compare with the green dash-dot-dot curve in Fig. 1).

B. Antiferromagnetic coupling

Now we direct our attention to the very small magnetic field behavior. There exists a very small region of the magnetic field where the total spin of electrons and the total spin of the magnetic ion are oriented parallel. We found this earlier in Ref. 15 for the zero magnetic field case. These results are now extended to nonzero magnetic field. This is made more clear in the upper inset of Fig. 3, where the crossing point of the two terms, the Zeeman energies of the magnetic ion (Δ_Z^{Mn}) and the exchange interaction (Δ_Z^{exc}), occurs at $\Omega_c=0.01$ (converted to $B\approx 0.1$ T for the considered system). This ferromagnetic (FM) coupling extends further, up to $\Omega_c=0.04$ (see the lower inset of Fig. 3).

It is worth noting that this ferromagnetic coupling is extended to a much larger magnetic field range (up to $\Omega_c=2.3$) if we move the magnetic ion to the center of the quantum dot (see Fig. 4). This can be understood as follows: When the magnetic ion is located at the center of the dot and the magnetic field is very small, the absolute value of Δ_Z^{Mn} always dominates over Δ_Z^{exc}. This is opposite of the case where the magnetic ion is located at $(0.5l_0,0)$. Recall that in Ref. 15 we found for zero field that the exchange Zeeman energy is minimum when the magnetic ion is at the center of the quantum dot and approximately zero at positions very far from the center of the quantum dot.

Figure 4 tells us that the magnetic field where the antiferromagnetic (AFM) coupling between electron and the magnetic ion starts depends on the position of the magnetic ion in the quantum dot. The system with the magnetic impurity located at $(l_0,0)$ exhibits an antiferromagnetic coupling for $\Omega_c\geq 0.1$, that is, larger than $\Omega_c=0.05$ in the case of $(0.5l_0,0)$.

We have discussed the appearance of antiferromagnetism in a three-electron quantum dot. Now we go back to the two

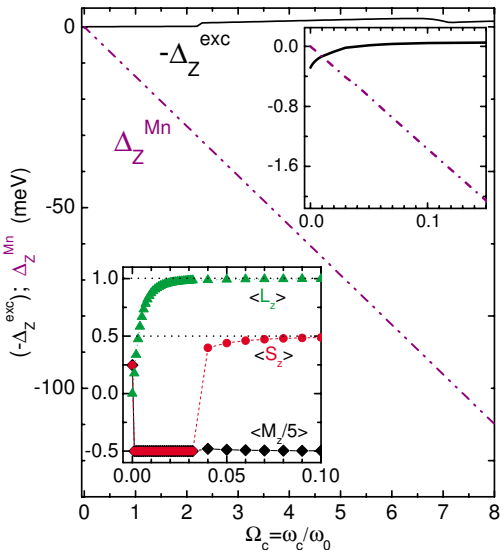

FIG. 3. (Color online) Zeeman energy of the magnetic ion and exchange interaction of a three-electron quantum dot with the magnetic ion located at $(0.5l_0,0)$ and the Coulomb strength $\lambda_C=0.5$. The upper inset is a zoom of the small magnetic field region and the lower one presents the averages of M_z, S_z, and L_z for the ground state at very small magnetic fields.

simpler cases with the number of electrons $N_e=1,2$ (see Fig. 5). Let us first discuss the results for $N_e=1$ as given in Fig. 5(a). The antiferromagnetic coupling between the electron and the magnetic ion starts at smaller magnetic field as the magnetic ion is moved. This is different from the previous results for $N_e=3$. The reason is as follows: For the quantum dot with a single electron, the electron tends to accommodate permanently the s shell with $\langle L_z\rangle=0$ [see the inset of Fig. 5(a)] in the ground state, while the exchange parameter

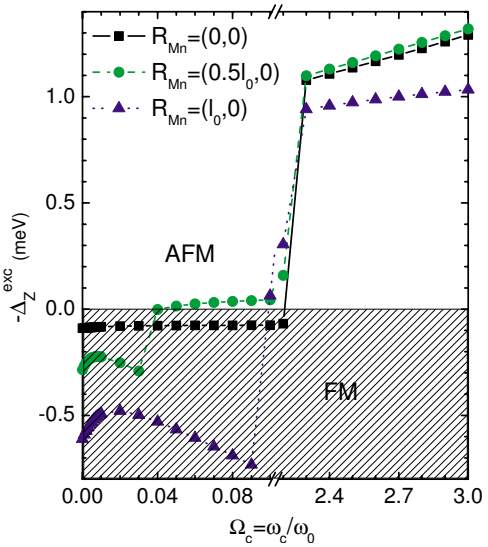

FIG. 4. (Color online) Exchange interaction of a three-electron quantum dot with the magnetic ion located at three different positions, $(0,0)$, $(0.5l_0,0)$, and $(l_0,0)$, for the Coulomb strength $\lambda_C=0.5$. The horizontal line at $\Delta_Z^{\mathrm{exc}}=0$ separates the Δ_Z^{exc} plane into FM and AFM regions.

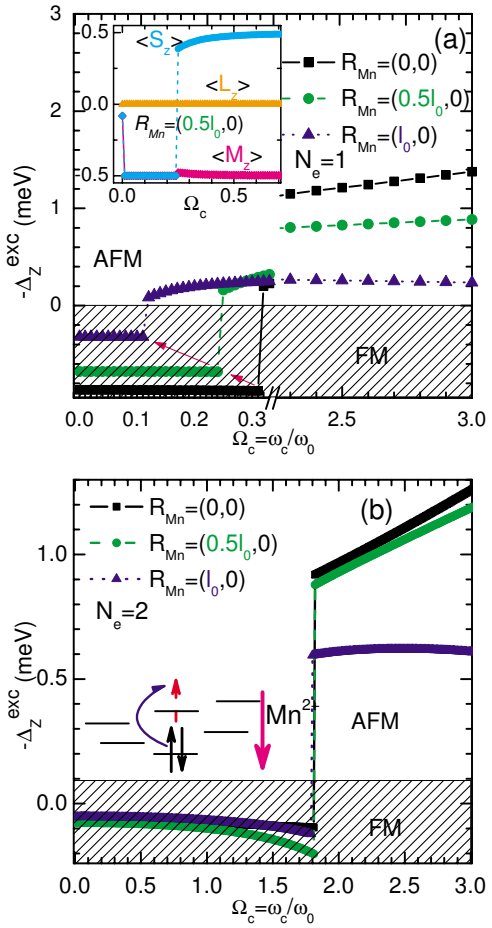

FIG. 5. (Color online) Exchange interaction of (a) a one-electron and (b) a two-electron quantum dot with the magnetic ion located at three different positions and the Coulomb strength $\lambda_C=0.5$. The inset of the upper plot shows the averages of the three quantities M_z, S_z, and L_z with the ion located at $(0.5l_0,0)$ at small magnetic fields. The horizontal line separates the plane into FM and AFM regions in both two plots. The schematic diagram in (b) explains why the exchange energy is almost zero in the case $N_e=2$.

in the s shell (J_{ss}) is found to be maximum right at the center of the quantum dot. Moving the magnetic ion away from the center of the dot, this J_{ss} is found to be smaller and as a consequence the exchange electron–Mn interaction becomes smaller than the electron Zeeman energy, leading to an antiferromagnetic coupling at smaller magnetic field.

The story of $N_e=2$ electrons [see Fig. 5(b)] is now interesting since the two electrons accommodate the s shell with spins antiparallel, making the total spin of the electron zero in the ground state with almost unit probability. This leads to zero contribution to the first term written in the last term in Eq. (2) for diagonal elements. Therefore, the main contribution (even very small) to the exchange energy is now expected to come from coupling with configurations where one of the electrons (spin down) stays in the s level and the other occupies a higher level [see the schematic diagram in Fig. 5(b)]. In this diagram, the magnetic ion is assumed to be located at the center of the dot with spin down $(-5/2)$. The coupling of the electron (spin up) in the s orbital with an electron from either of the p shell is zero. The only nonzero

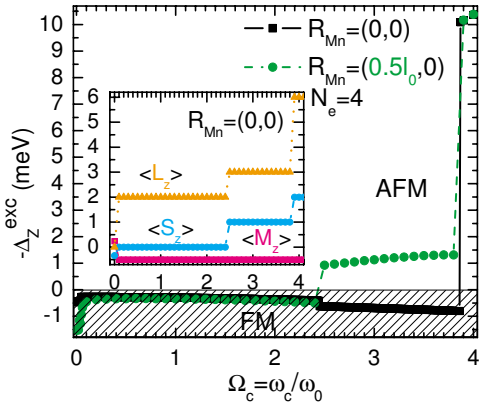

FIG. 6. (Color online) Exchange interaction of a four-electron quantum dot with the magnetic ion located at three different positions and the Coulomb strength $\lambda_C=0.2$. The horizontal line separates the plane into FM and AFM regions. The inset shows the total z projections of the M_z, S_z, and L_z of the electron system with the magnetic ion located at the center of the dot.

coupling is with an electron with the quantum numbers (1,0) of the d shell (as shown in the diagram. This quantum state would change if the ion is located away from the center of the dot) with the amount of about -10^{-2}. This picture remains valid until the magnetic field is high enough to excite one electron from the s shell to a higher quantum state, forming the ground state with two up spins antiferromagnetically coupling with the magnetic ion. For smaller Coulomb interaction strength, the antiferromagnetic behavior occurs at larger magnetic field since the two electrons repel each other less and consequently they stay longer antiparallel in the s shell.

From the $N_e=2$ result, we may ask a question: whether a four-electron quantum dot has similar properties since the numbers of electrons in both cases are even and one may have a situation where the total spin of the electrons is zero. Indeed, if the magnetic ion is located at the center of the quantum dot even though for $N_e=4$ the outer shell is half filled, this is possible as illustrated in Fig. 6, where the antiferromagnetic coupling occurs at $\Omega_c=3.87$, at which the total spin of the electrons reaches the maximum value $\langle S_z\rangle=2$. In this case, the first two electrons will occupy the s shell and the remaining two will occupy two of the five orbitals of the p and d shells. This picture holds at small magnetic field. However, there is a big difference in the exchange energy as compared to the previous case of $N_e=2$ where the ion is shifted away from the center of the dot, e.g., in this plot at $(0.5l_0,0)$. The exchange energy is much larger than the result obtained for $R_{\mathrm{Mn}}=(0,0)$ because when the ion is out of the center of the quantum dot, the two remaining electrons at higher orbitals have a nonzero contribution in the diagonal exchange elements dominating the exchange energy of the ground state. This is the reason why the antiferromagnetic transition occurs at smaller magnetic field ($\Omega_c=2.5$) as compared to the case where the ion is at the center of the dot ($\Omega_c=3.87$), although the pictures of the M_z and L_z transition in these cases are similar.

To complete the picture for few-electron quantum dot system, we will discuss the antiferromagnetic behavior for the

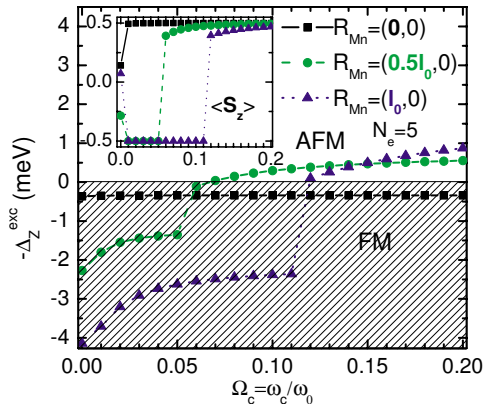

FIG. 7. (Color online) Exchange interaction of a five-electron quantum dot with the magnetic ion located at several positions and the Coulomb strength $\lambda_C=0.2$. The horizontal line separates the plane into FM and AFM regions. The inset shows S_z alone vs magnetic field.

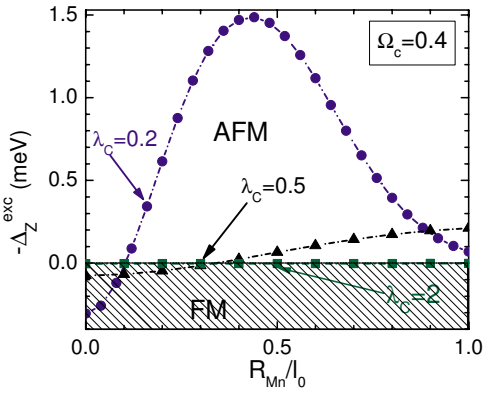

FIG. 8. (Color online) The magnetic ion position dependence of the exchange interaction of a three-electron quantum dot for Coulomb strengths $\lambda_C=0.2$, 0.5, and 2 at $\Omega_c=0.4$. The horizontal dotted line at $\Delta_Z^{\rm exc}=0$ separates the plane into FM and AFM regions.

system with the highest number of electrons, $N_e=5$, where we were able to obtain accurate numerical results. We focus on the small magnetic field region (see Fig. 7). For the magnetic ion at the center of the dot, the FM coupling is dominant in the shown magnetic field region because the diagonal exchange matrix elements dominate over the Zeeman energies of the electrons and of the magnetic ion. This is different for the cases with the magnetic ion displaced a bit from the center of the quantum dot. The ferromagnetic-antiferromagnetic (FM-AFM) transition occurs at $\Omega_c=0.07$ and $\Omega_c=0.12$ for $R_{\rm Mn}=(0.5l_0,0)$ and $R_{\rm Mn}=(l_0,0)$, respectively. It is similar to the cases for the system with $N_e=1,3$ due to the zero coupling between the orbitals from the p,d shell with the s orbital. To observe the AFM behavior for the system with the magnetic ion located at the center of the dot where the diagonal exchange elements are almost zero, it is crucial to include enough quantum orbitals (that rapidly increases the size of the Hamiltonian matrix, resulting in very time consuming calculations) so that one allows the electrons to jump to higher-energy levels and having parallel spins as previously shown for the case $N_e=4$ (see Fig. 6). In that case, the four-electron system exhibits an antiferromagnetic coupling with the magnetic ion at the magnetic field where the total z projection of the spin is maximum $S_z=2$. The system is strongly polarized. For the case $N_e=5$, up to $\Omega_c=0.2$, the total $S_z=0.5$ and the total $L_z=1$. The inset of Fig. 7 supports the AFM behavior for the out of center Mn as obtained in the main plot.

C. Phase diagram for the ferromagnetic-antiferromagnetic transition

Now we change the Coulomb interaction strength and explore the magnetic behavior as a function of the position of the magnetic ion. From Fig. 8, it is clear that when reducing the Coulomb interaction, the system undergoes a ferromagnetic-to-antiferromagnetic transition at gradually larger magnetic fields for Mn^{2+} positions that are closer to the center of the dot. We see that $-\Delta_Z^{\rm exc}$ has a peak structure with a maximum at some specific position of the magnetic ion; e.g., see the peak for the case $\lambda_C=0.2$ (blue full circles). However, it is certain that at high magnetic field, the system is always antiferromagnetic.

The FM-AFM phase diagram for a three-electron quantum dot in (λ_C,Ω_c) space is shown in Fig. 9 for two different positions of the magnetic ion. When the magnetic ion is at the center of the quantum dot (black curve with squares in Fig. 9), the critical magnetic field increases as the Coulomb interaction strength decreases. The reason is that increasing the Coulomb interaction helps the electrons to approach closer the magnetic ion and therefore the critical magnetic field for the system to transit to the antiferromagnetic phase decreases.

Now we move the magnetic ion away from the center of the quantum dot and we obtain the phase diagram as shown by the red curve (with solid circles) in Fig. 9. For $\lambda_C<0.4$, the stability of the FM phase with respect to an applied magnetic field is strongly reduced and a small magnetic field turns the three-electron system into the AFM phase. Note that for sufficient strong electron-electron interaction (i.e., $\lambda_C\geq 0.4$), we obtain practically the same FM-AFM phase diagram as for the case where the Mn ion is located at the

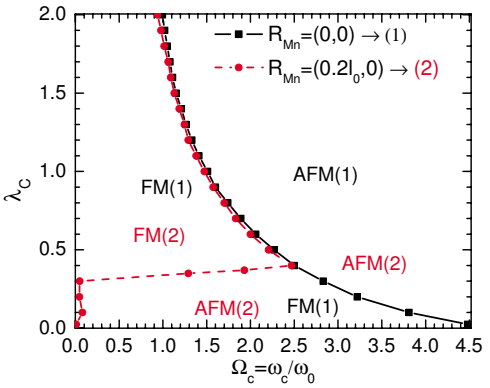

FIG. 9. (Color online) Phase diagram for the ferromagnetic-antiferromagnetic transition of a three-electron quantum dot with the magnetic ion located at (0,0) [black squares refer to (1)] and $(2l_0=5.29\ \text{Å},0)$ [red circles refer to (2)].

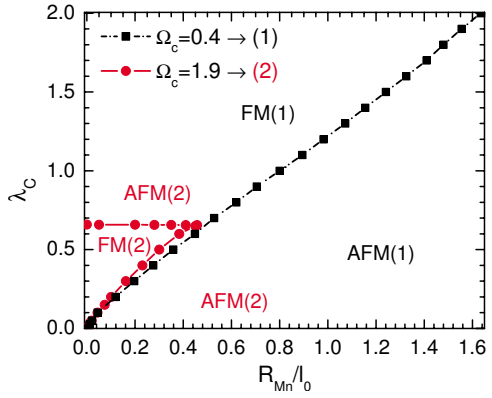

FIG. 10. (Color online) Phase diagram for ferromagnetic-antiferromagnetic transition of a three-electron quantum dot in an applied field of $\Omega_c=0.4$ [black squares refer to (1)] and $\Omega_c=1.9$ [red circles refer to (2)].

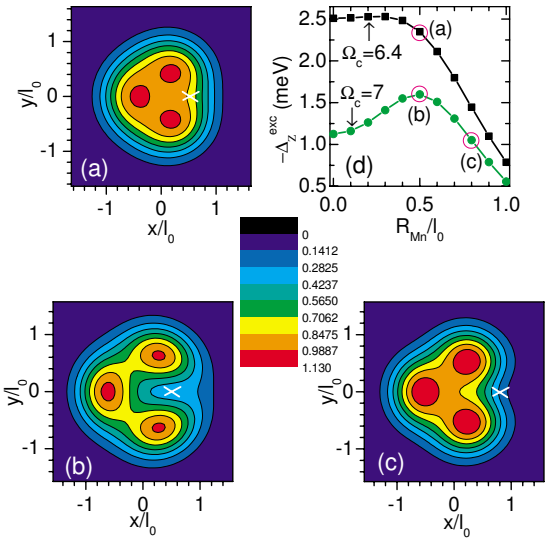

FIG. 11. (Color online) Radial density scaled by l_0^2 calculated for a three-electron quantum dot with the magnetic ion (white cross) located at $(0.5l_0,0)$ in (a) and (b) and at $(0.8l_0,0)$ in (c) when the Coulomb strength $\lambda_C=0.5$ in a magnetic field $\Omega_c=6.4$ [see (a)] and $\Omega_c=7$ [see (b) and (c)]. (d) is the magnetic ion position dependence of $-\Delta_Z^{\text{exc}}$ with the magenta circles indicating the respective calculated positions of the magnetic ion in (a)–(c). The red regions have the highest value of radial density.

center of the quantum dot. A remarkable re-entrant behavior is found in the region $0.3<\lambda_C<2$ and $0.9<\Omega_c<2.5$, where with increasing λ_C we go from an antiferromagnetic to a ferromagnetic phase and back to an antiferromagnetic phase. This unusual behavior is understood as follows: As the impurity is moved away from the center of the quantum dot, the exchange matrix will have many nonzero off-diagonal terms that lead to a smaller FM-AFM critical transition magnetic field. Now let us turn our attention to the region $\lambda_C<0.4$. For very small Coulomb interaction strength, the electrons will repel each other only weakly and are therefore pulled toward the magnetic ion (the nonzero exchange matrix elements increase strongly), resulting in a very small FM-AFM magnetic field. For $\lambda_C\geq 0.4$, the electrons become more strongly correlated and the critical field stays at about $\Delta\Omega_c \approx 0.02\div 0.07$ from the result for $R_{\text{Mn}}=0$. If one moves the ion further and further away from the center, the $\lambda_C\sim 0.4$ transition line moves to larger λ_C values. For example, for $\lambda_C=0.5$ and the magnetic ion located at $(0.5l_0,0)$, the FM-AFM critical transition occurs at $\Omega_c=0.08$, which is much smaller than 2.21 found for $R_{\text{Mn}}=(0.2l_0,0)$.

The dependence of the ferromagnetic-antiferromagnetic transition of a three-electron quantum dot system on the position of the magnetic ion is summarized in the phase diagram shown in Fig. 10 for two different magnetic fields $\Omega_c=0.4,1.9$. We can predict that with slightly larger (smaller) magnetic field, the slope of the curve will be larger (smaller). From Fig. 9, we already learned that the FM-AFM transition magnetic field is largest for the ion at the center of the quantum dot, as also seen in Fig. 10. The re-entrant behavior of the AFM phase as a function of λ_C is found for small R_{Mn}/l_0 values, i.e., when the Mn ion is not too far from the center of the quantum dot, in case the magnetic field is not too small. The critical point $(R_{\text{Mn}}/l_0,\lambda_C)=(0.457,0.656)$ for $\Omega_c=1.9$ moves down (up) with increasing (decreasing) magnetic field.

D. Density and correlation

In high magnetic field, the magnetic ion tends to attract electrons because they are oppositely polarized. Because the exchange interaction is small as compared to the Coulomb interaction, the electrons and magnetic ion are arranged in such a way that the electrons repel each other and also try to be as close to the magnetic ion as possible. This picture holds above the FM-AFM critical magnetic field.

To show this behavior explicitly, we studied the radial density and the radial pair-correlation functions. Their respective operators are defined as

$$\rho(\vec{r})=\sum_{i=1}^{N_e}\delta(\vec{r}-\vec{r_i}) \tag{10}$$

and

$$C_{\sigma\sigma'}(\vec{r},\vec{r}')=\sum_{i\neq j}^{N_e}\delta_{\sigma\sigma_i}\delta(\vec{r}-\vec{r_i})\delta_{\sigma'\sigma_j}\delta(\vec{r}'-\vec{r_j}). \tag{11}$$

We plot in Fig. 11 the radial density of a three-electron quantum dot that is polarized in high magnetic field for the case that the Coulomb strength is $\lambda_C=0.5$ and the magnetic ion is located at two different positions for two magnetic fields. The electrons and the magnetic ion are antiferromagnetically coupled. The strength of that coupling can be seen in Fig. 11(d), in which we plot the magnetic ion's position dependence of the exchange energy at two magnetic fields $\Omega_c=6.4$ and 7. Those magnetic fields are typical in the sense that the exchange term is found to be very large ($\Omega_c=6.4$) or the correlation between the electrons is very high ($\Omega_c=7$). Density plots are shown for R_{Mn} at $(0.5l_0,0)$ and $(0.8l_0,0)$. We observe three distinct peaks of maximum probability. They are found at $(-0.44l_0,0)$, $(0.22,0.44)l_0$, and $(0.22,-0.44)l_0$ in Fig. 11(a); $(-0.63l_0,0)$, $(0.26,0.63)l_0$, and

$(0.26,-0.63)l_0$ in Fig. 11(b); and $(-0.52l_0,0)$, $(0.26,0.52)l_0$, and $(0.26,-0.52)l_0$ in Fig. 11(c). These figures show clearly the interplay effect where the three electrons on one hand try to be close to the magnetic ion and on the other hand repel each other via the Coulomb potential energy. It results in the merging of the radial density such that the higher the exchange energy is, the larger is the merging of the local maxima in the electron density and the smaller are the correlations. Figure 11(d) gives an idea about the variation of $-\Delta_Z^{\text{exc}}$ with the position of the magnetic ion and that it reaches a maximum at $(0.5l_0,0)$ for $\Omega_c=7$. In Fig. 11(c), the three electrons are less attracted to the magnetic ion via the antiferromagnetic coupling as compared to that in Fig. 11(b). This is due to the fact that the $-\Delta_Z^{\text{exc}}$ for the case shown in Fig. 11(b) is larger than that in Fig. 11(c). The electrons are therefore found more correlated in the latter case, presented by the extended red region in Fig. 11(c). Thereby, the correlation between electrons in Fig. 11(c) is expected to be the highest and that in Fig. 11(a) to be the smallest.

The position of the magnetic ion affects the ground-state property as made clear in Fig. 12. We fix the spin state and the position of one electron (indicated by the orange arrow) and the position of the magnetic ion (white cross). The magnetic field is such that $\Omega_c=6.4$ in Fig. 12(a) and $\Omega_c=7$ in the others. It also reflects the fact that the system in Fig. 11(a) exhibits the smallest correlation as compared to the other two. This illustrates the point raised above about the density. At the magnetic field $\Omega_c=7$, the electrons are strongly polarized, resulting in the red regions of the up-up spin-pair-correlation function that tends to surround the magnetic ion. We see that the three electrons are most likely to localize around some specific positions defining a triangle with the three electrons at the three vertices while they are attracted to the magnetic ion. When we locate one electron at a position closer to the magnetic ion [see Fig. 12(b)], the two peaks decrease in amplitude as compared to those in Fig. 12(b).

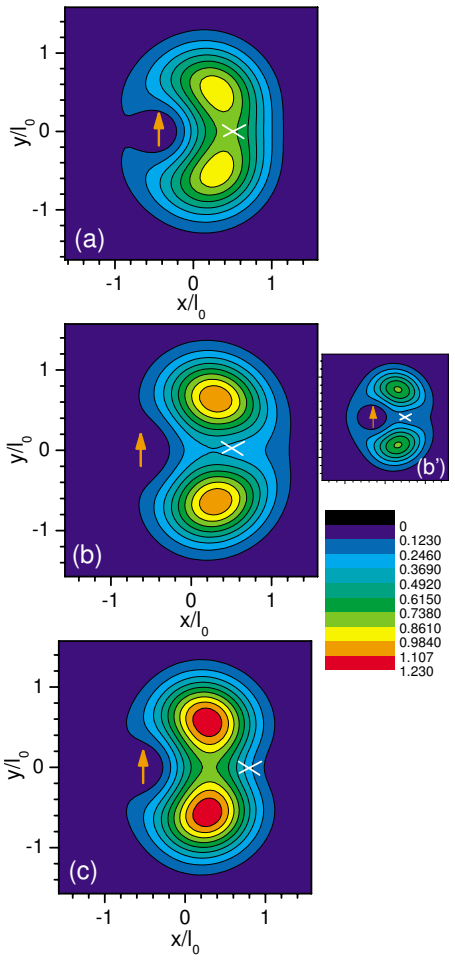

FIG. 12. (Color online) Spin-up pair-correlation functions scaled by l_0^4 calculated for the quantum dot in Fig. 11 where one electron (orange arrow) is pinned at one of the three most probable positions of the electrons as obtained in Fig. 11. It is at $(-0.44l_0,0)$ in (a) for Fig. 11(a), $(-0.63l_0,0)$ in (b) for Fig. 11(b), and $(-0.52l_0,0)$ in (c) for Fig. 11(c). (b′) The same correlation function for the case the position of the fixed electron is closer to the ion [at $(-0.3l_0,0)$] as compared to (b). The position of the magnetic ion is indicated by the white cross.

E. Addition energy

The addition energy (often called the chemical potential) is defined as the increase in the energy of the quantum dot system when an electron is added: $\mu_{N_e}=E_{\text{GS}}(N_e)-E_{\text{GS}}(N_e-1)$. This quantity can be measured experimentally; it is plotted in Fig. 13 as a function of the magnetic field.

There are several cusps appearing in the addition energy curves as a consequence of changes in the ground state. These changes are due to variations in the z projection of the total spin of the electrons and/or the z projection of the total angular momentum of the system when the magnetic field increases beyond some specific values. The presence of the magnetic ion leads to more cusps and the position of these cusps is also influenced by the number of electrons and the position of the magnetic ion. The cusps are from either of the two systems in the study. For instance, the green triangles in Fig. 13 are for $\mu_3=E_{\text{GS}}(N_e=3)-E_{\text{GS}}(N_e=2)$ has two cusps at $\Omega_c=2.6$ and $\Omega_c=3.4$. The cusp at the point $\Omega_c=2.6$ comes from the change in the configuration of the average of the total z-projection spin and the total z projection of angular momentum (S_z,L_z) of the two electrons in the quantum dot from (0,0) to (1,1). The other cusp $\Omega_c=3.4$ comes from the change in the phase of the three-electron quantum dot from (0.5,1) to (1.5,3). It is similar to the case for μ_4 (blue left-pointing triangles), where the cusp appears at $\Omega_c=3.4$. At this point, we observed a change from configuration (0,2) to (1,3). The remaining one, $\Omega_c=3.9$, is from the four-electron case when its configuration changes from (1,3) to (2,6).

F. Vortex structure: Many-body correlations

Another way to obtain information on the correlations that are present in the many-particle wave function is to investigate the vortex structure. At a vortex the many-body wave function is zero and is characterized by a change in phase of 2π when we go around this point.

The zeros of the wave function are similar to flux quanta when, e.g., the wave function corresponds to the order parameter in a superconductor. The fixed electrons and the zero

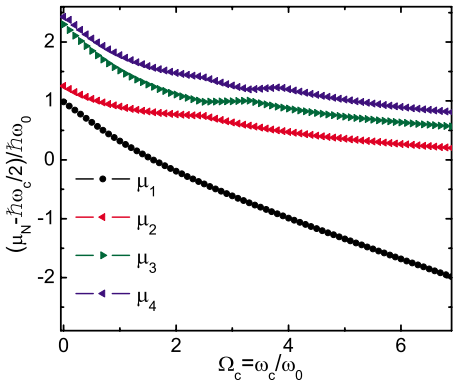

FIG. 13. (Color online) Addition energy for different numbers of electrons. The magnetic ion is located at $(0.41l_0,0)$ and the Coulomb interaction strength is $\lambda_C=0.2$.

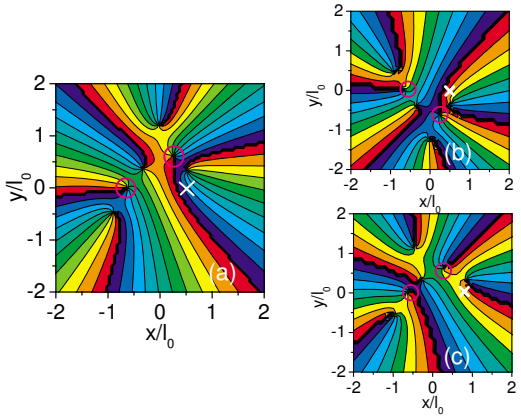

FIG. 14. (Color online) Contour plot for the phase of the reduced wave function of a three-electron quantum dot in magnetic field $\Omega_c=11$ with the magnetic ion (white cross) located at $(0.5l_0,0)$ in (a) and (b) and at $(0.8l_0,0)$ in (c) for Coulomb strength $\lambda_C=0.5$. Two fixed electrons (indicated by the two magenta circles) are located at the two peaks appearing in the radial density: $(-0.63l_0,0)$ and $(0.26,0.63)l_0$ in (a) and (c), and $(-0.63l_0,0)$ and $(0.26,-0.63)l_0$ in (b).

of the wave function follow closely the displaced electron and one may say that the electron plus its zero forms a composite-fermion object. The composite-fermion[13,17,18] (and references therein) is a collective quasiparticle that consists of one electron bound to an even number of vortices (flux quanta). The composite-fermion concept introduces a new type of quasiparticle that is used to understand the fractional quantum Hall effect in terms of the integer quantum Hall effect of these composite fermions.

To obtain the zeros of the wave function of the system with N_e electrons, we fix N_e-1 electrons at some positions inside the quantum dot and leave the remaining one free. The resulting reduced wave function gives the probability of finding the remaining electrons at different positions in the quantum dot. The zeros of this function are those points where the phase of the wave function changes by 2π. As an example, we investigate the situation of a three-electron quantum dot.

Figure 14 shows the vortex pictures of a three-electron quantum dot containing a magnetic ion located at positions (see the white cross) that are identical to its positions in Fig. 11(a). Two among three electrons are fixed at the respective peaks in the electron density. The red and black regions refer to the highest (2π) and lowest phases (0), respectively. Those plots show that there are always two vortices near the pinned electrons' positions. For example, the number of vortices pinned to each electron in the case $N_e=3$ at $\Omega_c=11$ is 2, describing the system at filling factor $\nu=\frac{N_e(N_e-1)}{2\langle L_z\rangle}\approx 1/3$. Note also that one of the vortices appears to be pinned at a position very close to the Mn ion.

We realize that moving the magnetic impurity to a different position changes the relative positions of the vortices that are pinned to the electrons with respect to one another, as shown in Figs. 14(a) and 14(c). As the electrons are antiferromagnetically coupling to the magnetic ion, this kind of movement consequently depends on the position of the magnetic ion.

In the case $\lambda_C=0.5$, we found that the average of the maximum z projection of the total angular momentum is $\langle L_z\rangle=9$ and the two vortices appear at the external field $\Omega_c=3.0$. Apparently, the larger λ_C is, the smaller is the Ω_c for which the first two vortices appear at the pinned electrons.

IV. ENERGY SPECTRUM

In the presence of an external magnetic field, the manyfold degeneracy of the energy spectrum of the system is lifted. Figure 15(a) illustrates that point for the case of three electrons. In the absence of the interaction between the electrons and the magnetic ion and in the absence of a magnetic field (blue squares), the energy spectrum is sevenfold degenerate for the first seven lowest energy levels. The next level is then fivefold degenerate, the next is sevenfold degenerate, and so on. The origin of this was explained in Ref. 15 and is due to the coupling of the electrons and the magnetic ion. When the magnetic field is different from zero [see the red circles in Fig. 15], the degeneracy is lifted. In the inset of Fig. 15 we plot $\langle M_z\rangle$ (magenta triangles) and $\langle S_z\rangle$ (dark blue triangles) as a function of magnetic field for the sixth level. The averages of $\langle M_z\rangle$ and $\langle S_z\rangle$ change abruptly as compared to those found for the ground-state energy; e.g., see Fig. 2. M_z and $\langle S_z\rangle$ of the sixth state jump between two different values, e.g., -1.5 and -2.5 for $\langle M_z\rangle$ and 0.5 and 1.5 for $\langle S_z\rangle$, as a function of the field. This is a consequence of the anticrossings of energy levels, as will be apparent later. The results for four- and five-electron quantum dots are also shown in Fig. 15. We see the degeneracy of 8, 6, 4, and 12 for the first 30 levels in the case $N_e=4$ and of 7, 5, 7, 5, 5. Level 30 has the same degeneracy with the next energy level beyond the first 30 for the case $N_e=5$ in $B=0$ T.

To have a clearer picture of the energy spectrum of the quantum dot system, we plot in Figs. 16–18 the magnetic field dependence of the first 120 energy levels for $N_e=1$, 2, and 3, respectively. The spectra at small magnetic fields are enlarged (see insets) to show the Zeeman splitting and the nearly linear behavior of the energy levels. Remember that this is due to the coupling of the electron spins with the magnetic ion spin. For $N_e=1$ the first two levels for $B=0$ are seven- and fivefold degenerate, respectively. (The sevenfold

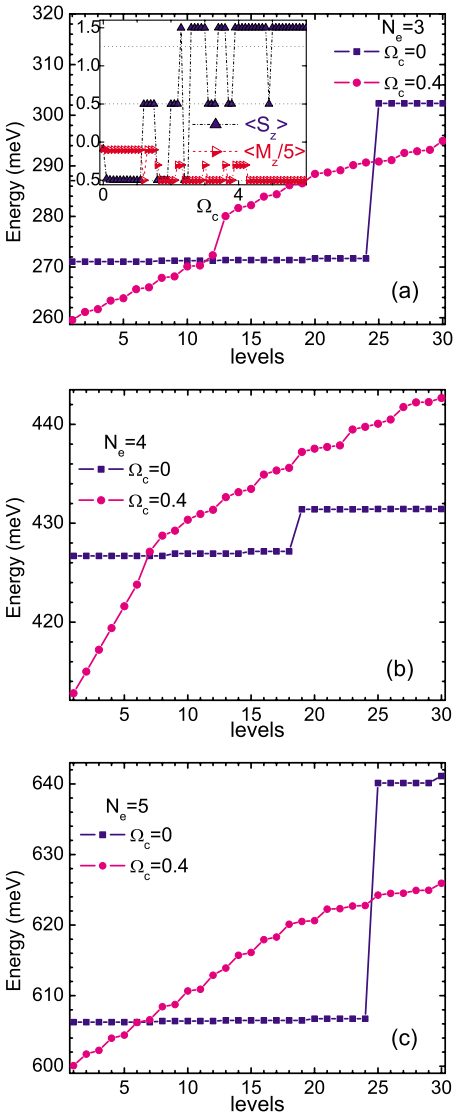

FIG. 15. (Color online) The energy spectra of the first 30 levels of the three- (top), four- (middle), and five-electron (bottom) quantum dots with the magnetic impurity located at $(0.5l_0,0)$. The Coulomb strength is $\lambda_C=0.5$ with magnetic fields $\Omega_c=0.0$ (blue squares) and $\Omega_c=0.4$ (magenta circles). The inset of the top figure shows the averages of M_z (dark blue triangles) and S_z (red triangles) as a function of Ω_c of the sixth energy level.

degeneracy is due to the ferromagnetic coupling of the s-shell electron spin 1/2 with the magnetic ion spin 5/2. The fivefold degeneracy is due to that of that electron now with spin $-1/2$ to the magnetic ion with spin 5/2.). A closer inspection (see Fig. 16) tells us that these 12 levels are exchange split into two bundles of 7 and 5 levels (inset of the inset of Fig. 16). Note that there is a first large energy gap at very small fields between the first 12 levels and the next 24 ones as seen in Fig. 16, while that kind of gap appears between the first 6 and the next 36 for $N_e=2$ (Fig. 17). For $N_e=3$ (Fig. 18), this kind of gap appears after the first 24 energy levels. The origin is the coupling of the third electron, which can reside at either two states of the p shell while the s shell is already fully filled, with the magnetic ion with six z components of the spin at very small fields, i.e., the in-

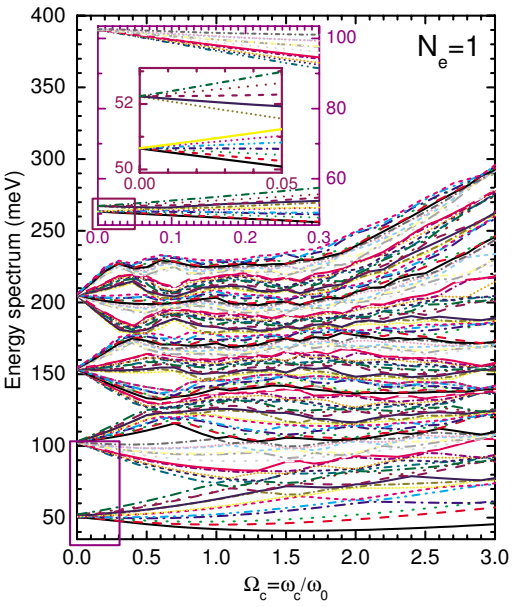

FIG. 16. (Color online) The magnetic field dependence of the energy spectrum (the first 120 levels are shown) of the one-electron quantum dot with the magnetic impurity located at $(0.5l_0,0)$ and $\lambda_C=0.5$. The inset is a zoom of the first 24 levels at low magnetic fields. The inset of the inset shows the first 12 levels; it is a zoom of the rectangular region.

trashell (p) exchange interaction. For $N_e=2$ the electron ground state corresponds with a filled s shell, i.e., $\langle S_z\rangle=0$. Therefore for $B=0$ only a sixfold degeneracy, as shown in Fig. 17, is found due to the z component of the Mn spin. The next level is eightfold degenerate at $B=0$ [the eightfold degeneracy comes from the ferromagnetic coupling of the two-electron system with total spin 1 to the magnetic ion with spin 5/2 (see the inset of the inset of Fig. 17)], etc.

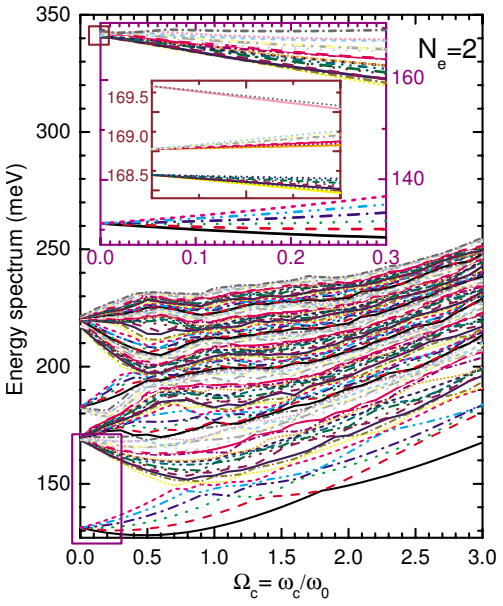

FIG. 17. (Color online) The same as Fig. 16 but now for the two-electron quantum dot. The inset of the inset is a zoom of the 7th–24th levels for magnetic field close to zero.

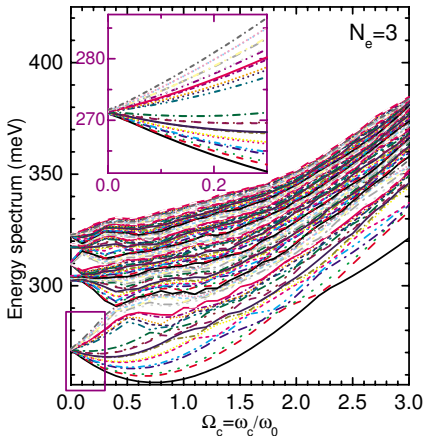

FIG. 18. (Color online) The same as Fig. 16 but now for the three-electron quantum dot.

With increasing magnetic field, we see that for $N_e=1$ there is periodically an opening of energy gaps in the spectrum. Similar energy gaps have been found earlier (as an example, see Ref. 19) for a quantum dot without a magnetic impurity and are a consequence of the electron with twofold spin degeneracy filling the equally gapped-energy single-particle quantum states with different sets of the radial and angular quantum numbers. Note that for $N_e=2,3$, these gaps have disappeared.

The spectra exhibit a lot of crossings and anticrossings. Their number has increased as compared to that in the quantum dot case without a magnetic ion because of the Zeeman splitting of the Mn spin. When the applied field increases, the gaps in the spectrum of $N_e=1$ are still open and appear more often than in the cases of $N_e=2,3$. Once again, we see a lot of cusps in the energy levels. That reminds us of the abrupt changes in the configuration of the system with magnetic field as discussed before for the ground state.

V. THERMODYNAMIC PROPERTIES

A. Magnetization and susceptibility

We first calculate the magnetization and susceptibility of the system: $M=-\partial E_{\mathrm{GS}}/\partial B$ and $\chi=\partial M/\partial B$ at zero temperature. The magnetization of a quantum dot with the magnetic ion located at $(0.5l_0,0)$ with $N_e=2,3$ electrons is plotted in Fig. 19. We see several jumps that are a consequence of changes in the ground state, e.g., changes in $\langle L_z\rangle$ (see Sec. IV). For example, the magnetization of the three-electron quantum dot as plotted in Fig. 19(b) for the case $\lambda_C=0.2$ and the magnetic ion at $(0.5l_0,0)$ has a step at $\Omega_c=3.3$. Consequently, the susceptibility also has a peak at $\Omega_c=3.3$. The same thing happens at $\Omega_c=1.4$, 4.1, and 6.8 for $\lambda_C=1.1$ in the magnetization and the susceptibility.

For nonzero temperature, the temperature dependence of the magnetization and susceptibility is defined by $M(T)=-\partial\langle E(T)\rangle/\partial B$ and $\chi(T)=\partial M(T)/\partial B$, respectively. The statistical average $\langle E(T)\rangle$ is calculated as

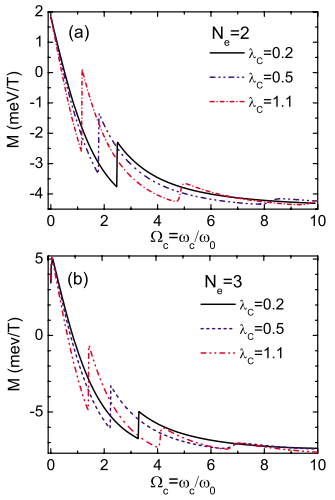

FIG. 19. (Color online) Magnetization of the ground state of the two- and three-electron quantum dots with the magnetic ion located at $(0.5l_0,0)$ for three values of the Coulomb strength: $\lambda_C=0.2$, 0.5, and 1.1.

$$\langle E(\lambda,T,R_{\mathrm{Mn}})\rangle=\frac{\sum_{\alpha=1}^{N_\alpha}E_\alpha e^{-E_\alpha/k_BT}}{\sum_{\alpha=1}^{N_\alpha}e^{-E_\alpha/k_BT}},\tag{12}$$

where the sum is over the energy levels as displayed in, e.g., Fig. 15.

These quantities are explored in Fig. 20 for $N_e=3$ and a few different temperatures (including the zero-temperature case). With increasing temperature, the jumps become smoother. A very low magnetic field peak shows up because for $T\neq 0$ we have $M\approx 0$ at $\Omega_c=0$.

B. Heat capacity

An important quantity that is related to the storage of energy is the heat capacity:

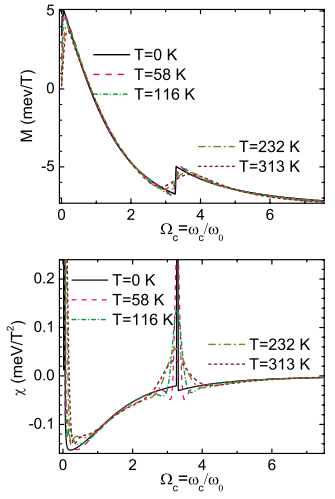

FIG. 20. (Color online) Temperature dependence of the magnetization and susceptibility for a three-electron quantum dot with the magnetic ion located at $(0.5l_0,0)$ and $\lambda_C=0.2$.

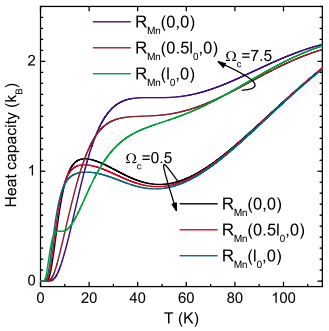

FIG. 21. (Color online) The heat capacity vs temperature of a three-electron quantum dot with the magnetic ion located at three different positions. The Coulomb interaction strength is 1.0 and the magnetic field Ω_c=0.5 (three lower curves) and 7.5 (three upper curves).

$$C_V(\lambda,T,R_{\mathrm{Mn}}) = \frac{\partial\langle E(\lambda,T,R_{\mathrm{Mn}})\rangle}{\partial T}. \tag{13}$$

The heat capacity is investigated as a function of the Coulomb strength λ, temperature T, magnetic field, and the position of the impurity R_{Mn}.

We plot in Fig. 21 the specific heat for two values of the magnetic field, i.e., Ω_c=0.5 and Ω_c=7.5, and three typical positions of the magnetic ion. For weak fields, the three electrons start to polarize. We see that the position of the main peak moves toward higher temperature as the magnetic ion is moved away but not too far from the center of the dot. For the high magnetic field case, the three electrons are strongly polarized and we see a different behavior in the shift of the main peak. This results from the change in the statistical average of the energy levels at different fields.

Now we examine the behavior of the heat capacity at a specific temperature as a function of magnetic field. Figures 22–24 are the plots of the magnetic field dependence of the heat capacity of three-electron (at two Coulomb interaction regimes) and four-electron quantum dots at some specific

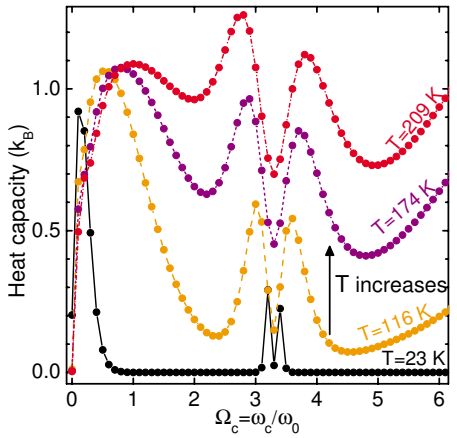

FIG. 22. (Color online) The heat capacity vs magnetic field of a three-electron quantum dot with the magnetic ion located at $(0.41l_0,0)$, λ_C=0.2, at several temperatures: 23, 116, 174, and 209 K.

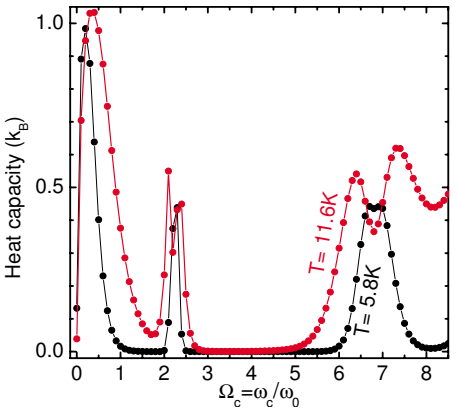

FIG. 23. (Color online) The heat capacity vs magnetic field of a three-electron quantum dot with the magnetic ion located at $(0.5l_0,0)$, λ_C=0.5, and the temperatures are 5.8 and 11.6 K.

temperatures and two different λ_C=0.2,0.5. The peak at small magnetic fields broadens and moves to higher fields with increasing temperature. The heat capacity exhibits a number of peaks and a clear minimum around, e.g., ω_c =3.4 as shown in Fig. 22. Recall that this field corresponds to a cusp in the energy versus magnetic field behavior as discussed previously in Sec. III A. At very low temperatures, this cusp still affects the heat capacity through the sharpness of the minimum as shown in the figure and this gradually becomes small at high temperatures. In Fig. 23, we see a very interesting behavior of the heat capacity at $\Omega_c \approx 2.3$: The single peak becomes a double peak as the temperature increases from T=5.8 K to T=11.6 K. This is due to the cusps now occurring around this field in the low-energy levels of the spectrum of the three-electron quantum dot system as observed in Fig. 18. Moreover, the structure of the heat capacity is more complex (more peaks) with increasing λ_C. This is made clear if one looks back at the previous discussion related to Figs. 1 and 2(a).

For the case N_e=4, the heat capacity exhibits more peaks as compared to the case N_e=3 and the behavior of the peaks with increasing temperature is also very different. Temperature affects the heat capacity of the system in the sense that it increases the peak values and separates them in magnetic field.

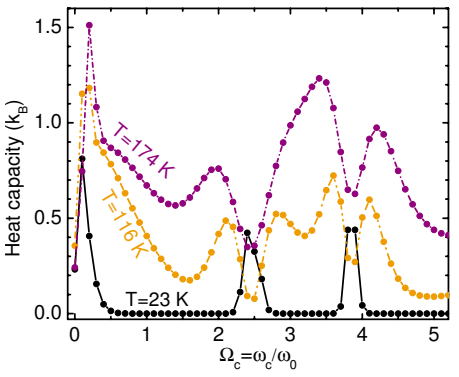

FIG. 24. (Color online) The heat capacity vs magnetic field of a four-electron quantum dot with the magnetic ion located at $(0.41l_0,0)$, λ_C=0.2 plotted for several temperatures.

The Coulomb interaction strength changes the structure of the magnetic field dependence of the heat capacity and is illustrated in Figs. 22 and 23. The peak of the heat capacity for the case with smaller Coulomb interaction strength appears at higher magnetic field as compared to the case with a larger one.

VI. DISCUSSIONS

Due to the presence of the magnetic ion (and electron-electron interaction), electrons in the ground state do not always completely polarize in the presence of an external magnetic field. The configurations are mixed, consisting of electrons with spins up and down. However for very large magnetic field, the magnetic ion tends to pull the electrons closer to the ion, forming a ringlike electron-density profile. These are the consequences of the interplay between several effects such as the Zeeman effect (on the electrons' and the magnetic ion's spins), the Coulomb repulsion, and the spin-exchange interaction. This competition results in a crossover from ferromagnetic-to-antiferromagnetic coupling between the electrons and the magnetic ion at some specific magnetic field. Interestingly, this effect is observed to appear at higher magnetic field when we move the magnetic ion farther from the origin of the quantum dot. A re-entrant behavior of the FM-AFM transition is found as function of the Coulomb interaction strength when the magnetic ion is moved out (but not too far) from the center of the quantum dot.

The energy levels exhibit cusps as a function of the magnetic field which correspond to changes in the configuration of the system as expressed by the values of $(\langle S_z\rangle, \langle L_z\rangle)$. These cusps move to lower magnetic field with increasing Coulomb interaction strength. The number of cusps increases with increasing number of electrons. These cusps show up in the addition energy.

The transformation of the electron system to those of composite fermions is studied. In high magnetic fields, the electrons attach an even number of quantized vortices, which we made clear by examining the many-body ground-state wave function in the presence of a magnetic ion. Unlike the case without a magnetic ion where all the vortices are tightly bound to the electrons, when we fix the electrons at different positions, the system of vortices stays pinned to the electrons and moves with the electrons but the relative positions of the vortices are modified.

The contribution of the local Zeeman splitting energy to the total energy of the system in large external fields is very small as compared to the contributions from the other parts. However, a slight movement of the position of the magnetic ion inside the quantum dot affects the result slightly.

With increasing applied magnetic field, each time the system jumps to a different $(\langle L_z\rangle, \langle S_z\rangle)$ configuration leads to the appearance of a peak in the thermodynamic quantities as, e.g., the susceptibility and the heat capacity. In the presence of the magnetic ion, the structure of peaks in the heat capacity changes with the position of the magnetic ion. As the temperature increases, these peaks split into two peaks and become smoother.

ACKNOWLEDGMENTS

This work was supported by FWO-Vl (Flemish Science Foundation), the EU Network of Excellence: SANDiE, and the Belgian Science Policy (IAP).

*nga.nguyen@ua.ac.be
†francois.peeters@ua.ac.be

[1] J. K. Furdyna, J. Appl. Phys. **64**, R29 (1988).
[2] D. L. Klein, R. Roth, A. K. L. Lim, A. P. Alivisatos, and P. L. McEuen, Nature (London) **389**, 699 (1997).
[3] Y. F. Chen, J. H. Huang, W. N. Lee, T. S. Chin, R. T. Huang, F. R. Chen, J. J. Kai, and H. C. Ku, Appl. Phys. Lett. **90**, 022505 (2007).
[4] K. Chang, J. B. Xia, and F. M. Peeters, Appl. Phys. Lett. **82**, 2661 (2003).
[5] A. O. Govorov, Phys. Rev. B **72**, 075358 (2005).
[6] Paul I. Archer, Steven A. Santangelo, and Daniel R. Gamelin, Nano Lett. **7**, 1037 (2007).
[7] J. Fernández-Rossier and L. Brey, Phys. Rev. Lett. **93**, 117201 (2004); L. Besombes, Y. Léger, L. Maingault, D. Ferrand, H. Mariette, and J. Cibert, *ibid.* **93**, 207403 (2004); Y. Léger, L. Besombes, L. Maingault, D. Ferrand, and H. Mariette, *ibid.* **95**, 047403 (2005); Y. Léger, L. Besombes, L. Maingault, D. Ferrand, and H. Mariette, Phys. Rev. B **72**, 241309(R) (2005);; L. Maingault, L. Besombes, Y. Léger, C. Bougerol, and H. Mariette, Appl. Phys. Lett. **89**, 193109 (2006).
[8] T. Schmidt, M. Scheibner, L. Worschech, A. Forchel, T. Slobodskyy, and L. W. Molenkamp, J. Appl. Phys. **100**, 123109 (2006).
[9] P. Wojnar, J. Suffczyński, K. Kowalik, A. Golnik, G. Karczewski, and J. Kossut, Phys. Rev. B **75**, 155301 (2007).
[10] J. Fernández-Rossier and Ramón Aguado, Phys. Rev. Lett. **98**, 106805 (2007).
[11] Y. Léger, L. Besombes, J. Fernández-Rossier, L. Maingault, and H. Mariette, Phys. Rev. Lett. **97**, 107401 (2006); L. Maingault, L. Besombes, Y. Léger, H. Mariette, and C. Bougerol, Phys. Status Solidi C **3**, 3992 (2006); M. M. Glazov, E. L. Ivchenko, L. Besombes, Y. Léger, L. Maingault, and H. Mariette, Phys. Rev. B **75**, 205313 (2007).
[12] Shun-Jen Cheng, Phys. Rev. B **72**, 235332 (2005).
[13] M. B. Tavernier, E. Anisimovas, F. M. Peeters, B. Szafran, J. Adamowski, and S. Bednarek, Phys. Rev. B **68**, 205305 (2003); M. B. Tavernier, E. Anisimovas, and F. M. Peeters, *ibid.* **70**, 155321 (2004); M. B. Tavernier, E. Anisimovas, and F. M. Peeters, *ibid.* **74**, 125305 (2006); T. Stopa, B. Szafran, M. B. Tavernier, and F. M. Peeters, *ibid.* **73**, 075315 (2006).
[14] Fanyao Qu and Pawel Hawrylak, Phys. Rev. Lett. **95**, 217206 (2005); **96**, 157201 (2006).
[15] Nga T. T. Nguyen and F. M. Peeters, Phys. Rev. B **76**, 045315 (2007).
[16] Ramin M. Abolfath, Pawel Hawrylak, and Igor Žutić, Phys. Rev. Lett. **98**, 207203 (2007).
[17] J. K. Jain, Phys. Rev. Lett. **63**, 199 (1989); Phys. Rev. B **41**, 7653 (1990); J. K. Jain, *ibid.* **42**, 9193(E) (1990).
[18] H. Saarikoski, A. Harju, M. J. Puska, and R. M. Nieminen, Phys. Rev. Lett. **93**, 116802 (2004).
[19] S. Tarucha, D. G. Austing, T. Honda, R. J. van der Hage, and L. P. Kouwenhoven, Phys. Rev. Lett. **77**, 3613 (1996).